J Clust Sci (2017) 28:2133–2146
DOI 10.1007/s10876-017-1208-y

ORIGINAL PAPER

A Facile Approach for Synthesis of a Novel WO_3–gC_3N_4/Pt–Sn–Os Catalyst and Its Application for Methanol Electro-oxidation

Mehrnoush Ghanbari[1] · Gholam Hossein Rounaghi[1] · Narges Ashraf[1] · Masoomeh Paydar[1] · Iman Razavipanah[1] · Mahdi Karimi-Nazarabad[1]

Received: 29 January 2017 / Published online: 10 April 2017

Abstract In the present work, a novel WO_3–gC_3N_4/Pt–Sn–Os catalyst was synthesized and used for fabrication of a modified electrode for electro-oxidation of methanol molecules. The WO_3–gC_3N_4 nanocomposite was transferred onto the surface of a glassy carbon electrode (GCE) and then, the surface of the modified electrode was potentiostatically coated with Pt–Sn–Os ternary alloy nanoparticles. The morphology of the prepared electrode (GCE/WO_3–gC_3N_4/Pt–Sn–Os), was characterized by scanning electron microscopy and energy dispersive X-ray spectroscopy. The electro-oxidation of methanol molecules on the surface of GC/WO_3–gC_3N_4/Pt–Sn–Os modified electrode was studied using various electrochemical methods such as cyclic voltammetry, chronoamperometry and electrochemical impedance spectroscopy (EIS). The charge transfer resistance and the double layer capacitance were determined by the EIS measurements. The electro-oxidation of methanol molecules was also investigated from kinetic point of view using the proposed modified electrode. The electrocatalytic performance of the modified electrode was also compared with the other constructed electrodes for methanol oxidation.

Keywords Electro-oxidation · Methanol · WO_3–gC_3N_4 nanocomposite · Pt–Sn–Os ternary alloy

Introduction

Fuel cells (FCs) are very valuable devices since they can directly convert chemical energy to electrical energy with a high efficiency [1]. Low-molecular weight alcohols are suitable candidates for use as fuel for fuel cells [2, 3]. Methanol is one

✉ Gholam Hossein Rounaghi
ronaghi@um.ac.ir; ghrounaghi@yahoo.com

[1] Department of Chemistry, Faculty of Sciences, Ferdowsi University of Mashhad, Mashhad, Iran

of the most promising fuels because of its relatively high activity [4], and nearly complete the electro-oxidation of its molecules to the final product of CO_2 [5]. Therefore, the direct methanol fuel cells (DMFCs) are of paramount importance.

Platinum has been applied as the most popular anodic electrocatalyst for oxidation of methanol molecules for many years [6–9]. Nevertheless, pure platinum has a high price and also it can be rapidly poisoned by the CO intermediate which is produced during methanol electro-oxidation [10]. To overcome these problems, some researches have been carried out to develop the catalyst for the electro-oxidation process of methanol molecules. An efficient way for decreasing the cost and improving the electrocatalytic properties of the electrodes, is alloying the Pt metal with a second metal such as Sn, Os, Al, Cr, Pd, Ru, Rh and Cu [11–19]. The other approach is using the nanocomposites materials for construction of the modified electrodes. Several investigations have shown that the nanocomposite materials can be used as catalysts for electro-oxidation of methanol molecules in fuel cells [20–24].

To improve the electrocatalytic activity of Pt–Sn–Os ternary alloy, we synthesized a WO_3–gC_3N_4 nanocomposite. Tungsten oxide (WO_3) which is an important n-type semiconductor with a small band gap (2.7–2.8 eV), has unique optical, electrical, and structural properties and a wide variety of applications in chemical and selective catalysis [25]. Many attempts have been done to improve the catalytic behavior of WO_3, such as morphology and size control [26, 27], noble metal deposition [28] and also its coupling with the other semiconductors. Among the above methods, the semiconductor coupling is one of the effective techniques. Various WO_3/semiconductor composites, such as CeO_2 [29], $CuBi_2O_4$ [30], Cu_2O [31] and Fe_2O_3 [32] have been prepared previously. The graphite carbon nitride (gC_3N_4) which is the most stable allotrope of carbon nitrides, has gained a significant interest due to its high thermal and chemical stability and also its application in solar energy conversion, photosynthesis, electrocatalysis and bio-imaging [33, 34].

The aim of the present work, is to enhance the methanol electro-oxidation efficiency by using WO_3–gC_3N_4 nanocomposite and Pt–Sn–Os ternary alloy catalyst in construction of a modified electrode. The experimental conditions and the results which are obtained in this research work, are presented and discussed in the next sections.

Experimental

Materials

$OsCl_3$ was purchased from Sigma-Aldrich Company. CH_3OH, $HClO_4$, H_2PtCl_6·$6H_2O$, $SnCl_4$·$5H_2O$, Na_2WO_4·$2H_2O$, melamine, urea and the other chemicals were purchased from Merck Chemical Company. All chemicals were of analytical grade and they used without any further purification. All solutions were prepared with deionized water.

Instrumentation

The electrochemical experiments were carried out at room temperature (25 °C) using a Potentiostat–Galvanostat (μ-AUTOLAB, ECO chemie) workstation which was equipped with an USB electrochemical interface and a driven NOVA software. A conventional three-electrode cell was used in this study. The three-electrode cell was consisted of an Ag/AgCl electrode (Azar Electrode Co., Urmia, Iran), a Pt wire electrode (Metrohm) and a glassy carbon electrode (Azar Electrode Co., Urmia, Iran) with a diameter of 2 mm.

X-ray diffraction (XRD) measurements were carried out with an X-ray diffractometer (Bruker/D8 ADVANCED) using Cu-K_α radiation ($\lambda = 1.54$ Å) and 0.05 degree step size. The size and shape of the WO_3 nanoparticles (NPs) were examined by a transmission electron microscopy (TEM, LEO 912 AB). The surface morphology and elemental analysis studies of the modified electrodes, were performed by scanning electron microscopy (SEM, LEO 1450 VP) and energy dispersive X-ray spectroscopy (EDX, Oxford 7353), respectively.

Synthesis of WO_3–gC_3N_4 Nanocomposite

Preparation of WO_3

For preparation of WO_3, at the first step, two aqueous solutions of HCl (4 mol L^{-1}) and $Na_2WO_4{\cdot}2H_2O$ (0.05 mol L^{-1}) were prepared. Then, 30 mL hydrochloric acid solution was added dropwise to 20 mL solution of sodium tungstate under stirring at room temperature until the pH of the solution became 2. The resulting solution was stirred for 1 h and then it was transferred into a Teflon tube in an autoclave at 60 °C. After 20 h, a yellow precipitate was formed in solution which was separated by centrifugation and washed several times with deionized water. Then, the precipitate was dried in a furnace at 250 °C for 3 h [25].

Preparation of gC_3N_4

For preparation of gC_3N_4, 2.5 g of melamine and 2.5 g of urea were well mixed using a mortar and the mixture was placed in a crucible [35] and heated in a furnace under certain calcination parameter settings as follows [36]: from room temperature to 300 °C (heating rate: 8 °C min^{-1}), from 300 to 500 °C (heating rate: 2 °C min^{-1}), from 500 to 550 °C (heating rate: 1 °C min^{-1}) and finally, it was heated at 550 °C for 2 h and then the crucible was cooled at room temperature. The product of the reaction was collected and grounded into a powder.

Preparation of WO_3–gC_3N_4

The WO_3–gC_3N_4 nanocomposite was synthesized by sonication method. The WO_3 and gC_3N_4 powders were mixed at 3:1 ratio in a mortar and the resultant mixed powder was mixed with 50 mL of deionized water and sonicated for 1 h. The suspended particles in the mixture, were separated by filtration and washed with

deionized water several times and then dried in a vacuum drying oven at 60 °C overnight [37].

Construction of the Modified Electrodes

The modified electrodes were constructed in three steps:

(a) First, the glassy carbon electrode (GCE) as a working electrode was polished with a slurry of 0.5 μm alumina and then rinsed with deionized water.
(b) 5.0 mg of WO_3–gC_3N_4 nanocomposite was dispersed in 5 mL deionized water for 20 min and then, 10 μL aliquot of the slurry was transferred onto the pre-polished GCE by using a sampler and dried under an infrared lamp for 10 min.
(c) The platinum based ternary alloy (i.e. Pt–Sn–Os) was electrochemically deposited at the surface of GC/WO_3–gC_3N_4 modified electrode from an aqueous solution containing 0.3 mol L^{-1} $HClO_4$, 2×10^{-3} mol L^{-1} H_2PtCl_6, 6×10^{-4} mol L^{-1} $SnCl_4$ and 4×10^{-4} mol L^{-1} $OsCl_3$ at a constant potential of −0.2 V versus Ag/AgCl electrode [38, 39].

A platinum based binary alloy (i.e. Pt–Sn) was also made according to the same procedure as step 3 with a solution containing 0.3 mol L^{-1} $HClO_4$, 2×10^{-3} mol L^{-1} H_2PtCl_6 and 6×10^{-4} mol L^{-1} $SnCl_4$. In addition, the GC/Pt–Sn–Os and GC/Pt–Sn electrodes were fabricated under the same experimental conditions, without adding any WO_3–gC_3N_4 nanocomposite on to their surface.

Results and Discussion

Characterizations of WO_3–gC_3N_4 Nanocomposite and Pt–Sn–Os Ternary Alloy

X-ray Diffraction Analysis

Figure 1, shows the XRD pattern of the WO_3, gC_3N_4 and WO_3–gC_3N_4 samples. The diffraction peaks of WO_3 nanoparticles can be assigned to both monoclinic (ICDD no. 00-043-1035) and orthorhombic (ICDD no. 00-020-1324) phases as the peaks overlap with each other [25]. The strong intensity and narrow width of WO_3 diffraction peaks, indicate that the resulting products are of high crystallinity. The XRD pattern illustrates no extra diffraction peaks, indicating that the WO_3 nanoparticles are prepared to a high level of purity. A typical XRD pattern of gC_3N_4 is shown in Fig. 1. In this XRD pattern, two pronounced diffraction peaks are observed at 12.8° and 27.6°. The presence of these two peaks, confirms that the gC_3N_4 is formed. The stronger peak at 27.6°, can be indexed to (002) diffraction plane for graphitic materials and is due to the interlayer stacking of the aromatic systems [40]. The broad diffraction peak at 12.8° is indexed as (100) in JCPDS 87-1526 [33]. The XRD pattern of WO_3–gC_3N_4 nanocomposite reveals the

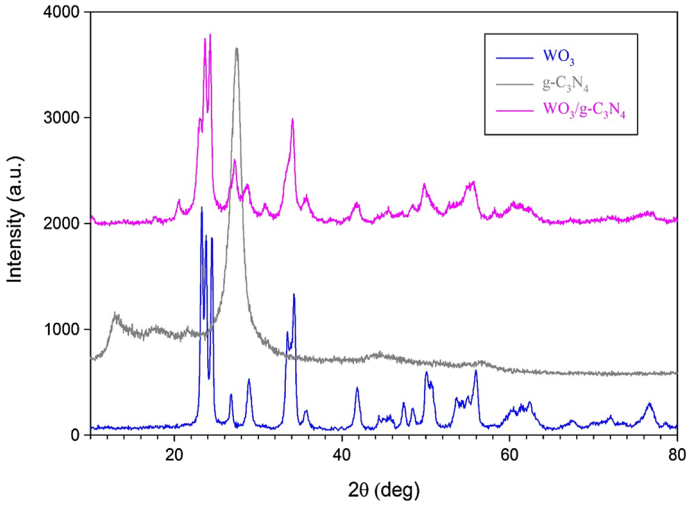

Fig. 1 X-ray diffraction patterns of the WO_3, gC_3N_4, and WO_3–gC_3N_4 samples

coexistence of WO_3 and gC_3N_4. The peaks assigned for gC_3N_4 in nanocomposite are weaker compared to those of the pure gC_3N_4.

Transmission Electron Microscopy Observation

The TEM image of the structure of the WO_3–gC_3N_4 nanocomposite is shown in Fig. 2. As is evident in this figure, the dark spots in the image, can be assigned to WO_3, whereas the grey area can be assigned to the presence of gC_3N_4 nanosheets.

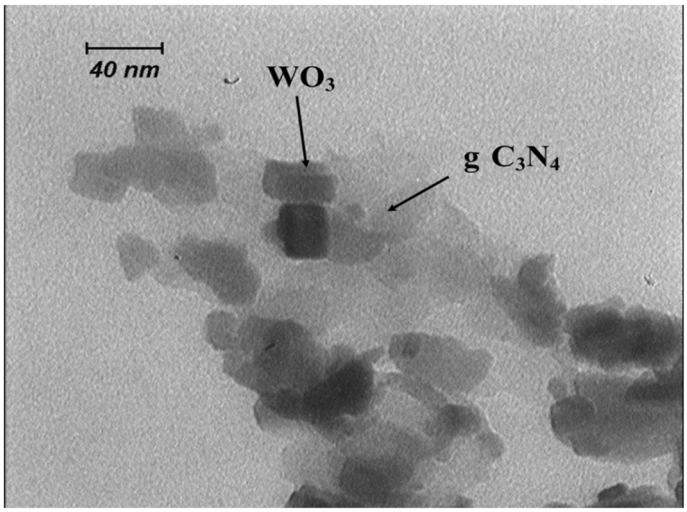

Fig. 2 TEM image of the WO_3–gC_3N_4 nanocomposite

The WO_3 nanoparticles are attached to the surface and the edge of the gC_3N_4 nanosheets and the WO_3 nanoparticles, cover the gC_3N_4 surface. The average particle size of WO_3 is 22 nm [25].

Scanning Electron Microscopy Observation and Energy Dispersive X-ray Investigation

Figure 3, demonstrates the scanning electron microscopic images of the bare GC, GC/WO_3–gC_3N_4 and GC/WO_3–gC_3N_4/Pt–Sn–Os electrodes. Figure 3a, shows the structure of the bare glassy carbon electrode surface immediately after polishing with a slurry of 0.5 μm alumina. Inspection of Fig. 3b, shows that the GCE surface is coated with a uniform coverage of WO_3–gC_3N_4 nanocomposite. Figure 3c, shows the SEM micrograph of the GCE/WO_3–gC_3N_4 surface after co-deposition of Pt–Sn–Os nanoparticles. As depicted in this figure, the Pt–Sn–Os nanoparticles with spherical morphology are formed throughout the surface of the WO_3–gC_3N_4 nanocomposite and it seems that the nanocomposite matrix acts as a good support and the Pt–Sn–Os nanoparticles are well dispersed on the surface of the GC/WO_3–gC_3N_4 electrode.

For further evaluation of immobilization of WO_3–gC_3N_4 nanocomposite and also co-deposition of Pt–Sn–Os ternary alloy at the surface of the glassy carbon electrode, energy dispersive X-ray (EDX) technique was employed. Figure 3d, indicates the EDX spectrum for WO_3–gC_3N_4 nanocomposite that reveals four high-intensity peaks at 1.4, 1.8, 8.4 and 9.6 keV corresponding to the presence of W and also, three separate peaks at 0.5, 0.4 and 0.3 keV representing the presence of O, N and C, respectively. The atomic ratio of the constituent atoms in nanocomposite, shows a pure sample with the ratio of 3:1 for WO_3:gC_3N_4. Also, Fig. 3e shows the EDX analysis results which are obtained for WO_3–gC_3N_4/Pt–Sn–Os electrocatalyst. As can be seen in this figure, all of the major peaks which are related to the WO_3–gC_3N_4 nanocomposite and Pt–Sn–Os ternary alloy are existed in the EDX spectrum that confirm that the Pt–Sn–Os nanoparticles are synthesized on the surface of the WO_3–gC_3N_4 nanocomposite.

Electrochemical Investigations

Cyclic Voltammetry

The electrocatalytic behavior of the catalysts was examined by cyclic voltammetry technique. Figure 4, shows the cyclic voltammograms for a solution containing 0.5 mol L^{-1} CH_3OH and 0.3 mol L^{-1} $HClO_4$ using the four constructed electrodes at a scan rate of 50 mV s^{-1}. Generally, the activity of a catalyst is evaluated using the values of the forward peak current density [41]. The graphical results in Fig. 4, show that the values of the peak current densities for methanol oxidation at the GC/WO_3–gC_3N_4/Pt–Sn–Os, GC/WO_3–gC_3N_4/Pt–Sn, GC/Pt–Sn–Os and GC/Pt–Sn electrodes are equal to 4.67, 3.19, 2.73 and 2.62 mA cm^{-2}, respectively. The results obtained in this study, display that the GC/WO_3–gC_3N_4/Pt–Sn–Os electrode, possess the highest forward peak current density. The enhanced electro-oxidation

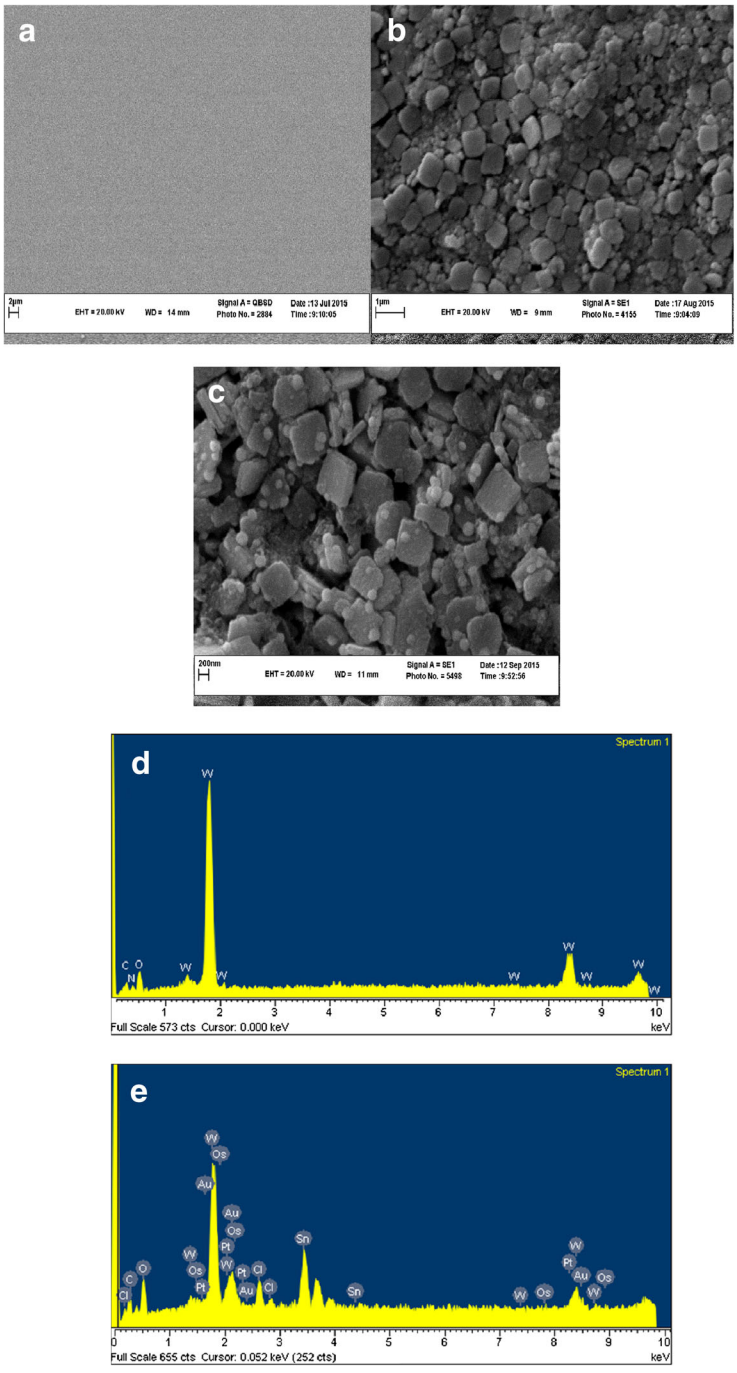

Fig. 3 SEM images of bare GC (**a**), GC/WO_3–gC_3N_4 (**b**), GC/WO_3–gC_3N_4/Pt–Sn–Os (**c**) electrodes, EDX spectra of WO_3–gC_3N_4 (**d**) and WO_3–gC_3N_4/Pt–Sn–Os (**e**)

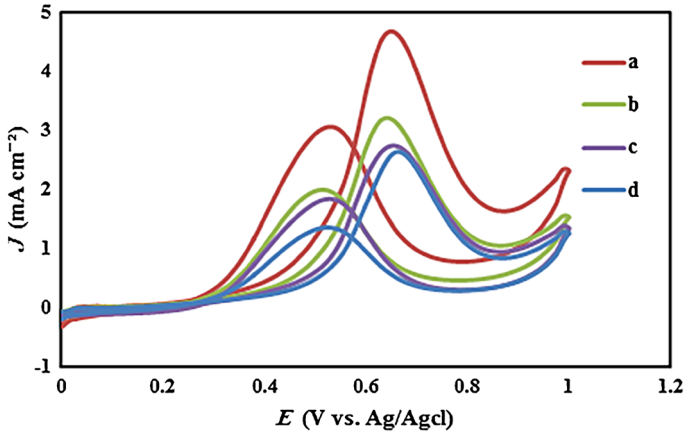

Fig. 4 Cyclic voltammograms of GC/WO_3–gC_3N_4/Pt–Sn–Os (*a*), GC/WO_3–gC_3N_4/Pt–Sn (*b*), GC/Pt–Sn–Os (*c*) and GC/Pt–Sn (*d*) electrodes in 0.5 mol L^{-1} CH_3OH + 0.3 mol L^{-1} $HClO_4$ solution at a scan rate of 50 mV s^{-1}, at room temperature

performance of the methanol molecules using the novel WO_3–gC_3N_4/Pt–Sn–Os catalyst can be attributed to the existence of the second and third metal particles (i.e. Sn and Os) in the catalyst and the synergistic effect between the ternary alloy nanoparticles and WO_3–gC_3N_4 nanocomposite.

Chronoamperometry

The chronoamperometry technique was employed for further investigation of the electrocatalytic performance of the GC/WO_3–gC_3N_4/Pt–Sn–Os, GC/WO_3–gC_3N_4/Pt–Sn, GC/Pt–Sn–Os and GC/Pt–Sn electrodes for oxidation of methanol

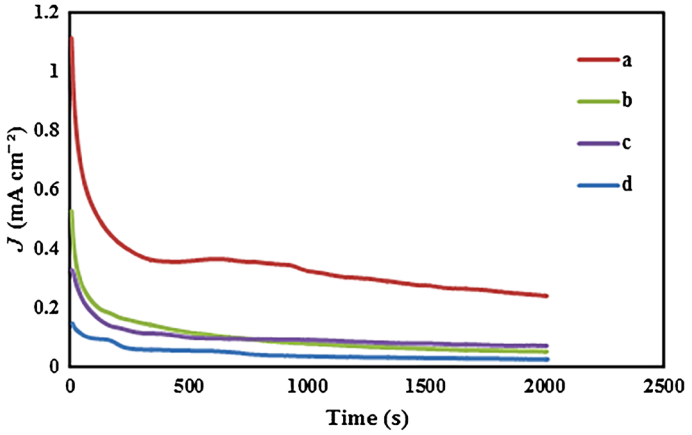

Fig. 5 Chronoamperograms of GC/WO_3–gC_3N_4/Pt–Sn–Os (*a*), GC/WO_3–gC_3N_4/Pt–Sn (*b*), GC/Pt–Sn–Os (*c*) and GC/Pt–Sn (*d*) electrodes in 0.5 mol L^{-1} CH_3OH + 0.3 mol L^{-1} $HClO_4$ solution at 0.55 V (vs. Ag/AgCl)

molecules. Figure 5, shows the chronoamperograms obtained using these modified electrodes at a fixed potential of +0.55 V in a solution containing 0.3 mol L^{-1} $HClO_4$ and 0.5 mol L^{-1} of methanol. As is evident in this figure, a gradual decay in the current density is observed with time in the case of these constructed electrodes. Nevertheless, during the whole time, the current density of the methanol molecules oxidation, is higher for the GC/WO_3–gC_3N_4/Pt–Sn–Os electrode compared to the other electrodes. The higher current density obtained with this electrode, is due to the presence of a greater number active sites at its surface which facilitate the electro-oxidation of the methanol molecules.

Electrochemical Impedance Spectroscopy

Electrochemical impedance spectroscopy (EIS) is a powerful technique, which is employed for studying of the interfacial electron-transfer processes and kinetics of the chemically modified electrodes [42]. Thus, the EIS technique was used to investigate the interface properties of GC/WO_3–gC_3N_4/Pt–Sn–Os, GC/Pt–Sn–Os, GC/WO_3–gC_3N_4/Pt–Sn, GC/Pt–Sn and bare GC electrodes. The electrochemical impedance spectroscopic measurements were carried out in the frequency range of 0.1–30,000 Hz with an amplitude of 10 mV with AC signals. Figure 6a, b, present the Nyquist plots and Bode plots using these electrodes which are obtained for a solution containing 0.3 mol L^{-1} $HClO_4$ and 0.5 mol L^{-1} CH_3OH at the open circuit potential (OCP), respectively. Figure 6c, shows an equivalent circuit which was used for analysis of the EIS results. This circuit includes the solution resistance (R_s), the charge transfer resistance (R_{ct}) and a constant phase element (CPE). A parallel combination of R_{ct} and CPE leads to the semicircles with different diameters, which their diameter equals the methanol oxidation charge transfer resistance. Constant phase element is used instead of the double layer capacitance (C_{dl}) in an equivalent circuit, due to the heterogeneity of the electrode surfaces [43]. The C_{dl} can be obtained by the following equation [44]:

$$C_{dl} = P^{\frac{1}{n}} R_{ct}^{\frac{1-n}{n}} \quad (1)$$

where P is the magnitude of CPE and n represents the deviation of the element from the ideal behaviour. The values of the equivalent circuit elements which are obtained by fitting the experimental results and they are derived by EIS spectrum analyzer software, are listed in Table 1. As can be seen from the graphical results in Fig. 6a, and the data in Table 1, the diameter of the semicircle for the GC/WO_3–gC_3N_4/Pt–Sn–Os electrode in Nyquist plots is smaller than those of the other electrodes, indicating that the charge transfer resistance of the GC/WO_3–gC_3N_4/Pt–Sn–Os electrode for methanol oxidation is lower than those of the other constructed electrodes. Generally, the lower the charge transfer resistance, results in a faster charge transfer rate at the surface of the electrode [45]. Also the impedance value (Z) at the frequency of 0.1 Hz for the GC/WO_3–gC_3N_4/Pt–Sn–Os electrode in Bode plots (Fig. 6b) is less than the other modified electrodes which is an evidence for a higher catalytic activity of the nanocomposite and ternary alloys electrode for electro-oxidation of methanol molecules.

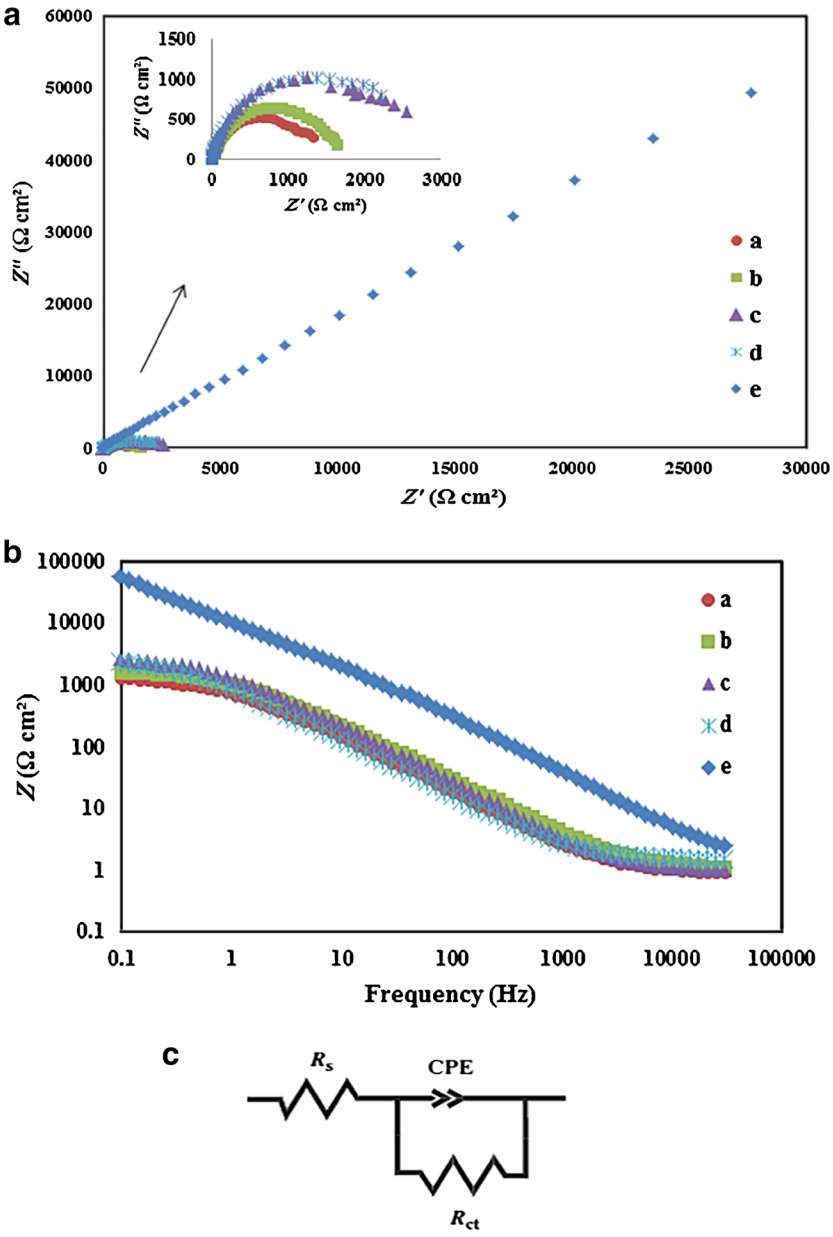

Fig. 6 **a** Nyquist plots of GC/WO_3–gC_3N_4/Pt–Sn–Os (*a*), GC/Pt–Sn–Os (*b*) GC/WO_3–gC_3N_4/Pt–Sn (*c*) and GC/Pt–Sn (*d*) and GC (*e*) electrodes at an open circuit potential, in 0.5 mol L^{-1} CH_3OH + 0.3 mol L^{-1} $HClO_4$ solution. The frequencies ranged from 30,000 to 0.1 Hz. **b** Bode plots of GC/WO_3–gC_3N_4/Pt–Sn–Os (*a*), GC/Pt–Sn–Os (*b*) GC/WO_3–gC_3N_4/Pt–Sn (*c*) and GC/Pt–Sn (*d*) and GC (*e*) electrodes at open circuit potential, in 0.5 mol L^{-1} CH_3OH + 0.3 mol L^{-1} $HClO_4$ solution. The frequencies ranged from 0.1 to 30,000 Hz. **c** The proposed equivalent circuit

Table 1 Circuit elements obtained for GC/WO_3–gC_3N_4/Pt–Sn–Os (a), GC/Pt–Sn–Os (b), GC/WO_3–gC_3N_4/Pt–Sn (c), GC/Pt–Sn (d) and GC (e) electrodes at open circuit potential, in a 0.5 mol L^{-1} CH_3OH + 0.3 mol L^{-1} $HClO_4$ solution

Sample	R_{ct} (Ω cm^2)	P (μF cm^{-2})	n	C_{dl} (μF cm^{-2})
a	1374.5	0.00023106	0.84516	1.87E−04
b	1658.1	0.00013059	0.8564	1.01E−04
c	2739.9	0.00018597	0.83006	1.62E−04
d	2815.5	0.00026643	0.84	2.52E−04
e	2.0608E05	2.0322E−05	0.82258	2.77E−05

Tafel Plots

The Tafel studies were carried out to evaluate the electrocatalytic activity of WO_3–gC_3N_4/Pt–Sn–Os, GC/WO_3–gC_3N_4/Pt–Sn and GC/Pt–Sn–Os electrodes for oxidation of methanol molecules from kinetic point of view. For this purpose, the exchange current densities (J_o) were measured using these modified electrodes. Figure 7, shows a typical Tafel curves for the above mentioned electrodes. The J_o values for the GC/WO_3–gC_3N_4/Pt–Sn–Os, GC/WO_3–gC_3N_4/Pt–Sn and GC/Pt–Sn–Os chemically modified electrodes, were calculated using the Tafel equation [46] and they were found to be: 1.26×10^{-5}, 6.3×10^{-6} and 5.25×10^{-6} mA cm^{-2}, respectively. Comparison of these values, indicates that the exchange current density for the GC/WO_3–gC_3N_4/Pt–Sn–Os electrode, is higher than the other electrodes. Therefore, it seems that the existence of WO_3–gC_3N_4 nanocomposite and Pt–Sn–Os ternary alloy at the surface of GC electrode, significantly accelerate the process electro-oxidation of methanol molecules.

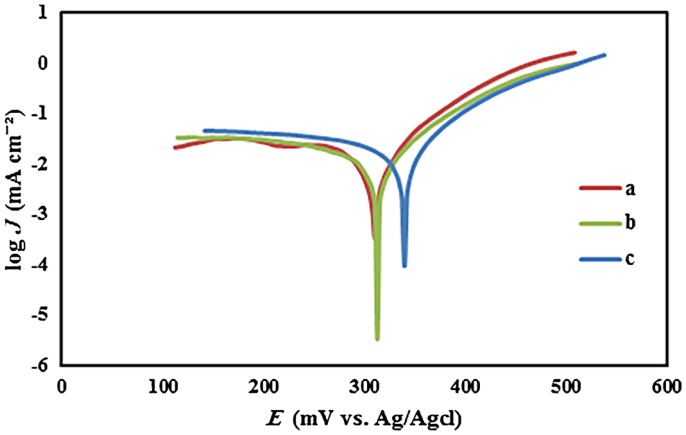

Fig. 7 Tafel plots of GC/WO_3–gC_3N_4/Pt–Sn–Os (*a*), GC/WO_3–gC_3N_4/Pt–Sn (*b*) and GC/Pt–Sn–Os (*c*) electrodes in 0.5 mol L^{-1} CH_3OH + 0.3 mol L^{-1} $HClO_4$ solution at a scan rate of 2 mV s^{-1}

Mechanism of the Methanol Electro-oxidation

The oxidation of methanol molecules at the electrode surface in the presence of Pt as an electrocatalyst has been widely studied [9, 18, 47]. The complete electro-oxidation of methanol molecules is expressed as [18]:

$$CH_3OH + H_2O \rightarrow CO_2 + 6H^+ + 6e^- \quad (2)$$

In general, the possible processes are described as follows:

$$Pt + CH_3OH \rightarrow Pt{-}CO_{ads} + 4H^+ + 4e^- \quad (3)$$

$$Pt + H_2O \rightarrow Pt{-}OH_{ads} + H^+ + e^- \quad (4)$$

$$Pt{-}CO_{ads} + Pt{-}OH_{ads} \rightarrow 2Pt + CO_2 + H^+ + e^- \quad (5)$$

The complete oxidation process of methanol (reaction 5), is carried out which results in a sharp increase in the oxidation peak current of methanol molecules.

Based on the obtained experimental results in this investigation, we can suggest that the enhanced electro-oxidation of the methanol molecules using the novel WO_3–gC_3N_4/Pt–Sn–Os catalyst can be attributed to the following effects:

The first effect is due to a bifunctional mechanism [48, 49]. According to this mechanism, the use of a second or a third metal, can lead to the formation of the hydroxy radicals by adsorption and dissociation of water molecules at more negative potentials which results in increasing the electro-oxidation of the CO molecules at the surface of the modified electrode. The second effect is the electronic effect [16, 50]. This mechanism is performed through the change of electronic structures of Pt by the presence of the alloyed metals and the nanocomposite, which can help to weaken the Pt–CO bond. Furthermore, addition of the nanocomposite as well as the second or the third element, results in a better Pt electrodeposition which produce a higher active sites at the surface of the modified electrode [50, 51].

Comparison of Electrocatalytic Performance of GC/WO_3–gC_3N_4/Pt–Sn–Os Constructed Electrode with the Other Pt-Modified Electrodes for Methanol Oxidation

The ratio of the forward anodic peak current ($I_{p,f}$) to the backward anodic peak current ($I_{p,b}$) can be used to evaluate the catalyst tolerance to poisoning. The results obtained in this study for the catalytic activity of the GC/WO_3–gC_3N_4/Pt–Sn–Os modified electrode towards methanol electro-oxidation are compared in Table 2 with those obtained for the recently reported Pt-modified electrodes. As evident in this table, the proposed electrode has a better or comparable ratio of the forward current to backward current ($I_{p,f}/I_{p,b}$) than the other modified Pt-electrodes. A higher $I_{p,f}/I_{p,b}$ value, implies the completeness electro-oxidation of the methanol molecules to CO_2 and less accumulation of the residual carbonaceous on the catalyst surface [19].

Table 2 Comparison between the ratio of forward current to backward current ($I_{p,f}/I_{p,b}$) of GC/WO_3–gC_3N_4/Pt–Sn–Os with recent constructed Pt-modified electrodes reported in the literature

No.	Composite electrode	$I_{p,f}/I_{p,b}$	References
1	Graphene nanoplate/Pt	1.21	[52]
2	Pt/graphene	1.071	[53]
3	Pt/C-20% polyaniline-para toluene sulfonic acid	0.8	[54]
4	Polyaniline/Pt microelectrodes	1.41	[55]
5	21% Pt/TiO_2 nanofibers	1.01	[56]
6	WO_3–gC_3N_4/Pt–Sn–Os	1.52	This work

Conclusions

The purpose of this research work, is construction of a modified electrode for electro-oxidation of methanol molecules in direct methanol fuel cells. In summary, a novel WO_3–gC_3N_4/Pt–Sn–Os electrocatalyst was prepared on the surface of a glassy carbon electrode and scanning electron microscopy and energy dispersive X-ray spectroscopy were employed for morphological study of the modified electrode surface. The electrochemical results obtained by this modified electrode, show an improved specific activity towards the methanol electro-oxidation compared with the other constructed electrodes. Moreover, comparison of the Toefl plots, shows that the GC/WO_3–gC_3N_4/Pt–Sn–Os modified electrode has a higher exchange current density (J_o) than the GC/WO_3–gC_3N_4/Pt–Sn and GC/Pt–Sn–Os electrodes. The experimental data show that the novel WO_3–gC_3N_4/Pt–Sn–Os catalyst can improve the performance of electro-oxidation of the methanol molecules as an anodic material in direct methanol fuel cells.

Acknowledgements The authors gratefully acknowledge the support of this work by Ferdowsi University of Mashhad, Mashhad, Iran (Grant No. 3/33748).

References

1. J. Yano, T. Shiraga, and A. Kitani (2008). *J. Solid State Electrochem.* **12**, 1179.
2. E. Antolini and E. Gonzalez (2010). *J. Power Sources* **195**, 3431.
3. K. Zhang, Z. Xiong, S. Li, B. Yan, J. Wang, and Y. Du (2017). *J. Alloys Compd.* **706**, 89.
4. S. Wasmus and A. Küver (1999). *J. Electroanal. Chem.* **461**, 14.
5. X. Ren, P. Zelenay, S. Thomas, J. Davey, and S. Gottesfeld (2000). *J. Power Sources* **86**, 111.
6. K. Shimazu, K. Uosaki, H. Kita, and Y. Nodasaka (1988). *J. Electroanal. Chem.* **256**, 481.
7. M. Watanabe, S. Saegusa, and P. Stonehart (1989). *J. Electroanal. Chem.* **271**, 213.
8. K. Shimazu, R. Inada, and H. Kita (1990). *J. Electroanal. Chem.* **284**, 523.
9. H. Razmi, E. Habibi, and H. Heidari (2008). *Electrochim. Acta* **53**, 8178.
10. C.-W. Kuo, B.-K. Chen, Y.-H. Tseng, T.-H. Hsieh, K.-S. Ho, T.-Y. Wu, and H.-R. Chen (2012). *J. Taiwan Inst. Chem. Eng.* **43**, 798.
11. M. Watanabe, Y. Furuuchi, and S. Motoo (1985). *J. Electroanal. Chem.* **191**, 367.
12. Y. Zhu and C.R. Cabrera (2001). *Electrochem. Solid-State Lett.* **4**, A45.
13. J. Huang, H. Yang, Q. Huang, Y. Tang, T. Lu, and D.L. Akins (2004). *J. Electrochem. Soc.* **151**, A1810.

14. M. Pournaghi-Azar and B. Habibi-A (2005). *J. Electroanal. Chem.* **580**, 23.
15. J.-S. Choi, W.S. Chung, H.Y. Ha, T.-H. Lim, I.-H. Oh, S.-A. Hong, and H.-I. Lee (2006). *J. Power Sources* **156**, 466.
16. F. Kadirgan, S. Beyhan, and T. Atilan (2009). *Int. J. Hydrogen Energ.* **34**, 4312.
17. Y.-J. Song, S.-B. Han, J.-M. Lee, and K.-W. Park (2009). *J. Alloys Compd.* **473**, 516.
18. I. Ávila-García, C. Ramírez, J.H. López, and E.A. Estrada (2010). *J. Alloys Compd.* **495**, 462.
19. F. Li, Y. Guo, M. Chen, H. Qiu, X. Sun, W. Wang, Y. Liu, and J. Gao (2013). *Int. J. Hydrogen Energ.* **38**, 14242.
20. E.S. Steigerwalt, G.A. Deluga, D.E. Cliffel, and C. Lukehart (2001). *J. Phys. Chem. B* **105**, 8097.
21. Y. Lin, X. Cui, C.H. Yen, and C.M. Wai (2005). *Langmuir* **21**, 11474.
22. L. Cao, F. Scheiba, C. Roth, F. Schweiger, C. Cremers, U. Stimming, H. Fuess, L. Chen, W. Zhu, and X. Qiu (2006). *Angew. Chem. Int. Ed.* **45**, 5315.
23. S. Palmero, A. Colina, E. Muñoz, A. Heras, V. Ruiz, and J. López-Palacios (2009). *Electrochem. Commun.* **11**, 122.
24. Y. Li, L. Tang, and J. Li (2009). *Electrochem. Commun.* **11**, 846.
25. M. Karimi-Nazarabad, E.K. Goharshadi, M.H. Entezari, and P. Nancarrow (2015). *Microfluid. Nanofluid.* **19**, 1191.
26. W. Morales, M. Cason, O. Aina, N.R. de Tacconi, and K. Rajeshwar (2008). *J. Am. Chem. Soc.* **130**, 6318.
27. F. Zheng, M. Zhang, and M. Guo (2013). *Thin Solid Films* **534**, 45.
28. R. Abe, H. Takami, N. Murakami, and B. Ohtani (2008). *J. Am. Chem. Soc.* **130**, 7780.
29. M.M. Natile, F. Tomaello, and A. Glisenti (2006). *Chem. Mater.* **18**, 3270.
30. T. Arai, M. Yanagida, Y. Konishi, Y. Iwasaki, H. Sugihara, and K. Sayama (2007). *J. Phys. Chem. C* **111**, 7574.
31. S. Wei, Y. Ma, Y. Chen, L. Liu, Y. Liu, and Z. Shao (2011). *J. Hazard. Mater.* **194**, 243.
32. P. Zhao, C.X. Kronawitter, X. Yang, J. Fu, and B.E. Koel (2014). *Phys. Chem. Chem. Phys.* **16**, 1327.
33. X. Bai, L. Wang, R. Zong, and Y. Zhu (2013). *J. Phys. Chem. C* **117**, 9952.
34. M. Zhu, C. Zhai, M. Sun, Y. Hu, B. Yan, and Y. Du (2017). *Appl. Catal. B: Environ.* **203**, 108.
35. R.C. Dante, P. Martín-Ramos, A. Correa-Guimaraes, and J. Martín-Gil (2011). *Mater. Chem. Phys.* **130**, 1094.
36. J. Xu, Y. Wang, and Y. Zhu (2013). *Langmuir* **29**, 10566.
37. T. Ohno, N. Murakami, T. Koyanagi, and Y. Yang (2014). *J. CO_2 Utilization* **6**, 17.
38. S. Golabi and A. Nozad (2003). *Electroanalysis* **15**, 278.
39. B. Habibi, M. Pournaghi-Azar, H. Abdolmohammad-Zadeh, and H. Razmi (2009). *Int. J. Hydrogen Energ.* **34**, 2880.
40. A. Thomas, A. Fischer, F. Goettmann, M. Antonietti, J.-O. Müller, R. Schlögl, and J. M. Carlsson (2008). *J. Mater. Chem.* **18**, 4893.
41. X. Zhang, G. Xia, C. Huang, and Y. Wang (2013). *Int. J. Hydrogen Energ.* **38**, 8909.
42. E. Katz and I. Willner (2003). *Electroanalysis* **15**, 913.
43. M.E. Orazem, and B. Tribollet, *Electrochemical impedance spectroscopy*, John Wiley & Sons, 2011.
44. B. Hirschorn, M. E. Orazem, B. Tribollet, V. Vivier, I. Frateur, and M. Musiani (2010). *Electrochim. Acta* **55**, 6218.
45. D. Soundararajan, J. Park, K. Kim, and J. Ko (2012). *Curr. Appl. Phys.* **12**, 854.
46. J. Wang, *Analytical electrochemistry*, John Wiley & Sons, 2006.
47. M. Zhiani, B. Rezaei, and J. Jalili (2010). *Int. J. Hydrogen Energ.* **35**, 9298.
48. R. Raman, A. Shukla, A. Gayen, M. Hegde, K. Priolkar, P. Sarode, and S. Emura (2006). *J. Power Sources* **157**, 45.
49. S. Lu, C. Zhang, and Y. Liu (2011). *Int. J. Hydrogen Energ.* **36**, 1939.
50. U.B. Demirci (2007). *J. Power Sources* **173**, 11.
51. B. Hasa, E. Kalamaras, E.I. Papaioannou, L. Sygellou, and A. Katsaounis (2013). *Int. J. Hydrogen Energ.* **38**, 15395.
52. H. Huang, H. Chen, D. Sun, and X. Wang (2012). *J. Power Sources* **204**, 46.
53. K. Kakaei and M. Zhiani (2013). *J. Power Sources* **225**, 356.
54. H. Gharibi, M. Amani, H. Pahlavanzadeh, and M. Kazemeini (2013). *Electrochim. Acta* **97**, 216.
55. R. Yan and B. Jin (2014). *Electrochim. Acta* **115**, 449.
56. Y. Zheng, H. Chen, Y. Dai, N. Zhang, W. Zhao, S. Wang, Y. Lou, Y. Li, and Y. Sun (2015). *Electrochim. Acta* **178**, 74.